Journal of
Materials Chemistry A

Materials for energy and sustainability

Accepted Manuscript

This article can be cited before page numbers have been issued, to do this please use: J. Kim, G. Kim, J. Y. Kim, S. Kim, H. Lee, Y. Eom, I. H. Jung and H. Kim, *J. Mater. Chem. A*, 2026, DOI: 10.1039/D6TA00020G.

ROYAL SOCIETY OF CHEMISTRY

rsc.li/materials-a

View Article Online
DOI: 10.1039/D6TA00020G

ARTICLE

Synergistic Enhancement of Strength and Ductility in Crosslinked Polymer Binders for High-Stability Silicon Anodes in Lithium-Ion Batteries

Received 00th January 20xx,
Accepted 00th January 20xx

DOI: 10.1039/x0xx00000x

Junho Kim†[a], Gyuri Kim†[b], Ji Young Kim[a], Sohyun Kim[a], Hyunjun Lee[b], Youngho Eom[b], In Hwan Jung*[b] and Hansu Kim*[a]

Crosslinking of the polymer binder is a powerful approach to suppress volume changes of Si-anode in lithium-ion batteries. However, this curing system is predominantly effective for soft-type flexible polymeric backbones and not for hard-type rigid polymeric structures due to the excessive brittleness they induce. In this study, a highly efficient crosslinking system applicable to hard-type polyimide (PI) and polyamide imidazole (PAID) was developed via crosslinking-induced flexibilization of polymeric backbone. We newly found that the chemical reaction of PI and PAID with oxirane-functionalized polyhedral oligomeric silsesquioxane (POSS) induces crosslinking while surprisingly softening the polymer backbone, which is an effect that has not been previously reported. As a result, the crosslinking prevents excessive stiffening of the polymer backbone, which consequently enhances the ductility, strength, and toughness of the binder, thereby improving the overall mechanical stability of Si-based anodes during repeated charging/discharging cycles. In addition, the crosslinking generates additional hydroxyl groups within the polymer binders, which enhances their interfacial interactions with Si nanoparticles. This unique crosslinking system exhibited markedly higher reversible capacity and significantly improved cycle stability than the non-cured binders over 200 cycles at a rate of 0.2 C. It shows strong potential for universal applicability across hard-type polymeric architectures.

Introduction

Lithium-ion batteries (LIBs) have gained traction as electrical energy storage systems for portable electronic devices and electric vehicles [1-3]. As the demand for higher-capacity and longer-duration LIBs continues to increase, the development of LIBs exhibiting high energy density has become essential [4]. However, graphite anode materials widely used polyimides in commercialized LIBs has nearly reached their theoretical capacity of 372 mAh g^{-1} (LiC_6) [4-6]. To address this theoretical limitation, various anode materials have been proposed for next-generation LIBs. Among these, Si is particularly promising as an anode material owing to its high theoretical capacity of 3579 mAh g^{-1} ($Li_{15}Si_4$) [7, 8]. However, Si undergoes intrinsically large volume expansion and contraction (up to 300%) during lithiation and delithiation, resulting in the mechanical degradation of Si particles, loss of electrical contact in the electrode, delamination of composite electrode layer from Cu current collector, and formation of thick solid electrolyte interphase layer, eventually compromising long-term capacity retention in Si anodes [9-11]. To address these challenges, various polymer binders have been introduced for Si anodes to effectively manage the volume expansion/contraction of Si anodes during cycling and enhance the adhesion between the active materials and current collectorr [12-14]. Recent studies have highlighted diverse binder design strategies for Si-based anodes, including supramolecular interactions, multifunctional network structures, and molecularly engineered polymer systems, to improve electrode integrity and cycling stability.[15-18] Notably, polyimides (PIs) have recently shown a bright future as a potential binder for Si anodes owing to their superior thermal stability, chemical resistance, mechanical strength and adhesive properties [19, 20]. Li et al. demonstrated that carbonyl PI binders enhance cycle stability of Si anode compared with those utilizing polyvinylidene fluoride and carboxymethyl cellulose / styrene-butadiene rubber binders, which was attributed to the high mechanical strength resulting from the rigid PI backbone and strong intermolecular interactions such as π-π stacking and hydrogen bonding [21]. Xu et al. reported a carboxylated PI binder capable of forming efficient hydrogen bonding with the Si particles, resulting in enhanced cycle performance and exhibiting a discharge capacity of 809 mAh g^{-1} after 100 cycles; however, Si anodes using simple PI binder exhibited a rapid decrease in capacity to 293 mAh g^{-1} after only 45 cycles [22]. Aminated PI also demonstrated that the additional amino groups enhanced both the adhesion to Si particles as well as the backbone strength via the formation of a ladder-type polymer

[a] Department of Energy Engineering, Hanyang University, 17 Haengdang-dong Seongdong-gu, Seoul 04763, Republic of Korea
[b] Department of Organic and Nano Engineering, and Human-Tech Convergence Program, Hanyang University, 222 Wangsimni-ro, Seongdong-gu, Seoul 04763, Republic of Korea.
† These authors contributed equally to this work
Supplementary Information available: [details of any supplementary information available should be included here]. See DOI: 10.1039/x0xx00000x

View Article Online
DOI: 10.1039/D5TA09986C

structure, thereby significantly enhancing the capacity retention of Si anodes over 200 cycles [23].

Despite the promising binding properties of PIs, the intermolecular interactions relying on physical attraction such as π-π stacking and hydrogen bonding between polymer backbones remain susceptible to long-term durability against the repeated volume changes experienced by Si anodes. To address this issue, a chemical cross-linking system ideally offers a better solution for reducing the morphological deformation of Si anodes during cycling due to its covalent bonding nature [24, 25]. Recently, Liang et al. reported that azide-based crosslinking of polyimide binders improves the mechanical rigidity of NCM cathodes by forming a three-dimensional polymer network[26]. However, unlike Si anodes, NCM cathodes do not undergo significant volumetric expansion, and thus issues related to crosslinking-induced brittleness have not been raised. In contrast, for high-volume-change electrodes such as Si anodes, chemical crosslinking of a rigid, hard-type PI backbone can render the polymer binder excessively brittle, thereby introducing additional challenges for long-term stability under repeated volume changes[27, 28]. Consequently, chemical crosslinking systems in Si anodes are predominantly applied to soft-type binders based on aliphatic polymer backbone chains [29, 30].

In this study, we newly found that the crosslinking of aromatic polyamide imidazole (PAID) (PI family) and polyimide (PI) polymers with oxirane-functionalized polyhedral oligomeric silsesquioxane (POSS) surprisingly flexibilizes the PI backbone chains, forming a three-dimensional polymer network that does not become excessively rigid. POSS is characterized by a spherical structure composed of relatively flexible Si-O bonds containing multifunctional pendant groups on its surface, enabling highly effective crosslinking, even in small quantities [31, 32]. In particular, the introduction of octafunctional oxirane terminal groups on these pendant groups increases the reactivity of POSS toward nucleophilic amino groups [33, 34]. Therefore, PI and PAID, both of which contain nucleophilic nitrogen atoms, undergo highly effective crosslinking reactions with oxirane-functionalized POSS. Notably, these curing reactions inhibit heterocyclic ring formation in the polymer backbone chains, preventing both PI and PAID from becoming excessively rigid as a ladder structure, thereby softening the backbones of both polymers while forming a 3D network structure. Stress–strain measurements demonstrated that POSS crosslinking increased both the strength and ductility of the polymer binders, indicating the concurrent enhancement of stronger intermolecular interactions and more flexible polymer chains. Furthermore, peel tests, density functional theory (DFT) calculations, and surface and interfacial cutting analysis system (SAICAS) evaluations indicated that the newly developed POSS crosslinked PI and PAID binders (denoted as PI-P and PAID-P, respectively) exhibit significantly improved mechanical properties compared with those without the POSS crosslinker. Therefore, Si anode based on crosslinking-induced flexibilization demonstrated a substantially enhanced initial discharge capacity of 2820 mAh g^{-1} and capacity retention of 66% (1881 mAh g^{-1}) after 200 cycles compared with those utilizing the pristine PAID binder. Our proposed crosslinking system is remarkably effective in enhancing the ductility, strength and toughness of the poly binder, which is key to minimizing the structural deformation of the polymer caused by large volume changes of the Si anode during cycling.

Experimental

Materials

4,4'-oxydianiline (98%), Pyromellitic dianhydride (98%), and 3,3'-Diaminobenzidine (98%) were purchased from Alfa Aesar. Dimethylformamide (DMF; anhydrous, 99.8%) and 1-Methyl-2-pyrrolidinone (NMP; anhydrous, 99.5%) were purchased from Sigma-Aldrich. Silicon powder (crystalline, APS l<50 nm, 98%) was purchased from Thermo Fisher Scientific Inc. All chemicals were used without further purification. Super P carbon (Commercial vendor) was stored at 80 ℃ before use.

Preparation of polymer binders

Polymerization of polyimide (PI): 4,4'-oxydianiline (2.29 mmol, 459 mg) was dissolved in DMF (10.0 ml) under nitrogen atmosphere. Pyromellitic dianhydride (2.29 mmol, 500 mg) dissolved in DMF (30.0 ml) was added dropwise into the solution at 0 ℃ and the mixture was stirred at room temperature overnight. The reaction mixture was recrystallized from diethyl ether and water, and subsequently dried under vacuum conditions at room temperature. The resulting polymer was obtained as a yellow solid (Yield, 97%).

Polymerization of polyamide imidazole (PAID): 3,3'-Diaminobenzidine (2.29 mmol, 491 mg) was dissolved in DMF (10.0 ml) under nitrogen atmosphere. Pyromellitic dianhydride (2.29 mmol, 500 mg) dissolved in DMF (30.0 ml) was added dropwise into the solution at 0 ℃ and the mixture was stirred at room temperature overnight. The reaction mixture was recrystallized from diethyl ether and water, and subsequently dried under vacuum conditions at room temperature. The polymer obtained was a brown solid (Yield, 98%).

Characterization of the binder and electrode materials

Fourier-transform infrared (FT-IR) spectra were recorded employing a Nicolet 6700 FT-IR Spectrometer (Thermo Scientific). Gel permeation chromatography (GPC) was conducted at room temperature utilizing DMF with 0.05 M LiBr as the eluent. DFT calculations were conducted using the Gaussian 16 program and 6-31G(d,p) basis set to obtain binding energies following the equation:

$$E_{bind} = E_{AB} - (E_A + E_B) \quad (1)$$

[E_{bind}:the binding energy between components A and B, E_{AB}: the total energy of the combined system, E_A: component A, E_B: component B].

Peel tests and SAICAS for the adhesion of Si electrodes to the Cu current collector were measured at 3 kgf load-cell employing the Instron 5966 Tester (Instron Engineering Co., Ltd.) and SAICAS EN-EX (Daipla Wintes). The crosslinking-induced flexibilization of the PI films was investigated using dynamic mechanical analysis (DMA, DMA 850, TA instruments, USA). To elucidate the enhancement of the network structure,

View Article Online
DOI: 10.1039/D6TA00020C

temperature ramp tests were conducted from 30 to 500 °C at a heating rate of 5 °C min^{-1} using rectangular specimens (17.5 mm × 12.7 mm × 2 mm). The measurements were performed at a frequency of 1.0 Hz, with a strain of 0.05% and a preload force of 0.1 N.

Nanoindentation measurements were conducted using a nanoindenter (Step500 NHT3/MCT3, Anton Paar) to evaluate the mechanical properties of the electrodes. The reduced modulus (Er) and hardness (H) were calculated from the load–displacement curves using the Oliver–Pharr method.

The morphology and microstructure of the active materials were examined via field-emission scanning electron microscopy (FESEM, JEOLJSM-7000F, Akishima, Japan). Electrochemical impedance spectroscopy (EIS) measurements were conducted using an impedance analyzing potentiostat (VSP-300, BioLogic) conFig.d with an altering current (AC) amplitude of 10 mV and a frequency range from 1 mHz to 1 MHz. XPS was measured using a Nexsa X-ray photoelectron spectrometer (Thermo Fisher Scientific) equipped with a monochromated Al Kα X-ray source. Mercury intrusion porosimetry (MIP) measurements were carried out using an AutoPore V9620 (Micromeritics) to analyze the pore structure of the electrodes.

Electrochemical measurements

The synthesized *p*-PAID powder was dissolved in 15 wt% NMP to prepare the electrodes. The Si anodes were fabricated using a slurry composed of 60% nano silicon, 20% Super P, 19.8% binder, and 0.2% POSS dissolved in NMP and coated onto Cu foil using a doctor blade. The cast slurries were heated at 80 °C for 1 h and subsequently dried at 200 °C under vacuum conditions for 2 h. The active mass loading of all electrodes was approximately 0.50 ± 0.1 mg cm^{-2} based on the Si content. The Si anode was cut into 1.1 cm^2 pieces to serve as working electrodes, and coin cells (CR2032 types) were assembled with polypropylene separators and Li counter electrode. The electrolyte consisted of 1 M $LiPF_6$ in EC/EMC = 3/7 (v/v) and 5.0 wt% fluoroethylene carbonate (Panax Etec Co. Ltd. South Korea) were added to the coin cells. All the coin cells were fabricated in an Ar-purged glove box. Electrochemical tests were conducted at the constant current-constant voltage (CC-CV) mode over the voltage range of 0.005–1.5 V (vs. Li/Li^+) at room temperature and a current density of 0.2–1 C (1 C = 3,579 mAh g^{-1}).

Results and Discussion

Synthesis and Characterization of Materials

PI and PAID polymers were synthesized following established procedures [35]. The synthesized polymers were characterized via GPC utilizing a DMF eluent with 0.05 M LiBr at room temperature [36]. The number-average molecular weight ($\overline{\mathbf{M}_n}$) of the PI and PAID polymers were 4526 and 2629 kDa, respectively, and the corresponding weight-average molecular weight ($\overline{\mathbf{M}_w}$) were 5400 and 7672 kDa, respectively (Fig. S1-S2). Both polymer binders exhibited molecular weights suitable for use as binders for Si anodes. These high molecular weights in addition

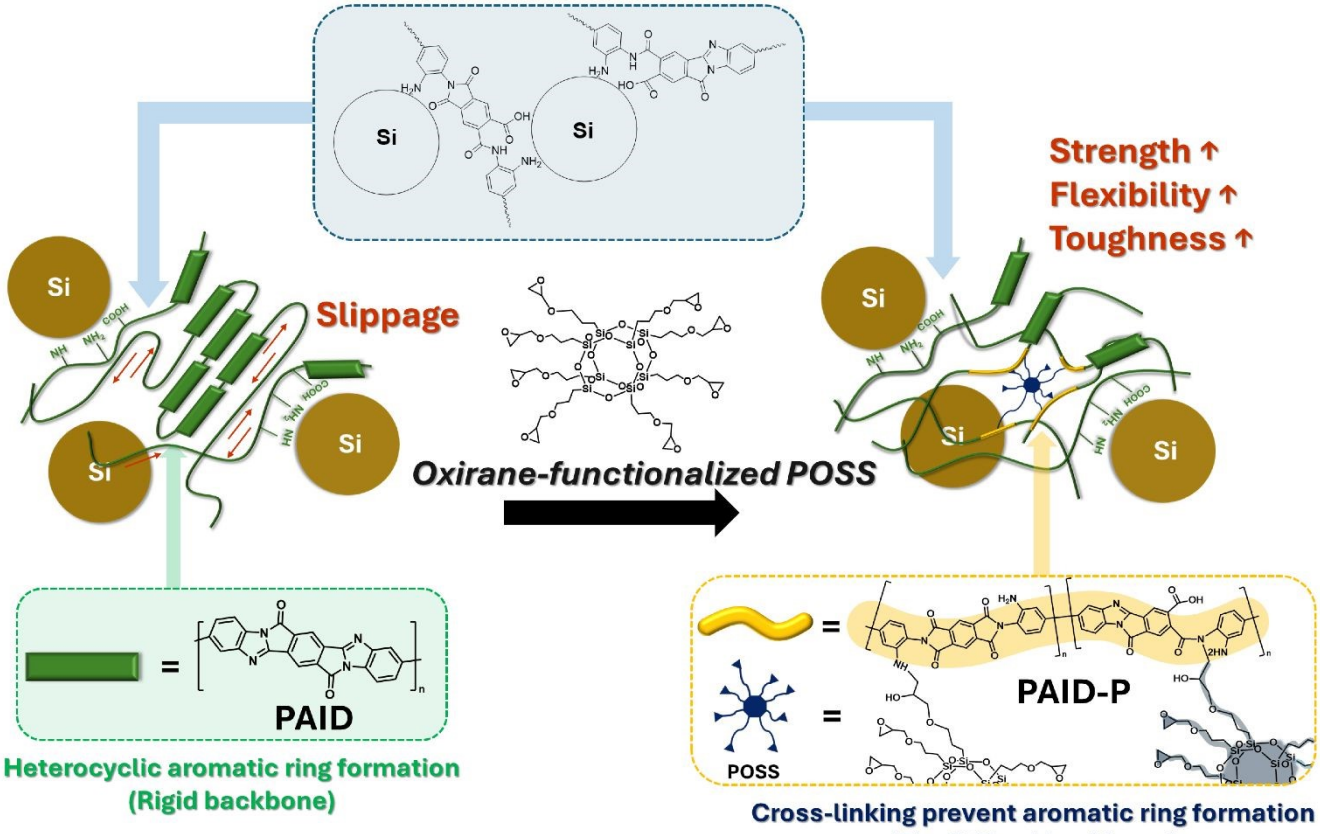

Scheme 1 Schematic description of POSS crosslinked PAID (PAID-P) binder for Si anode.

View Article Online
DOI: 10.1039/D6TA00020G

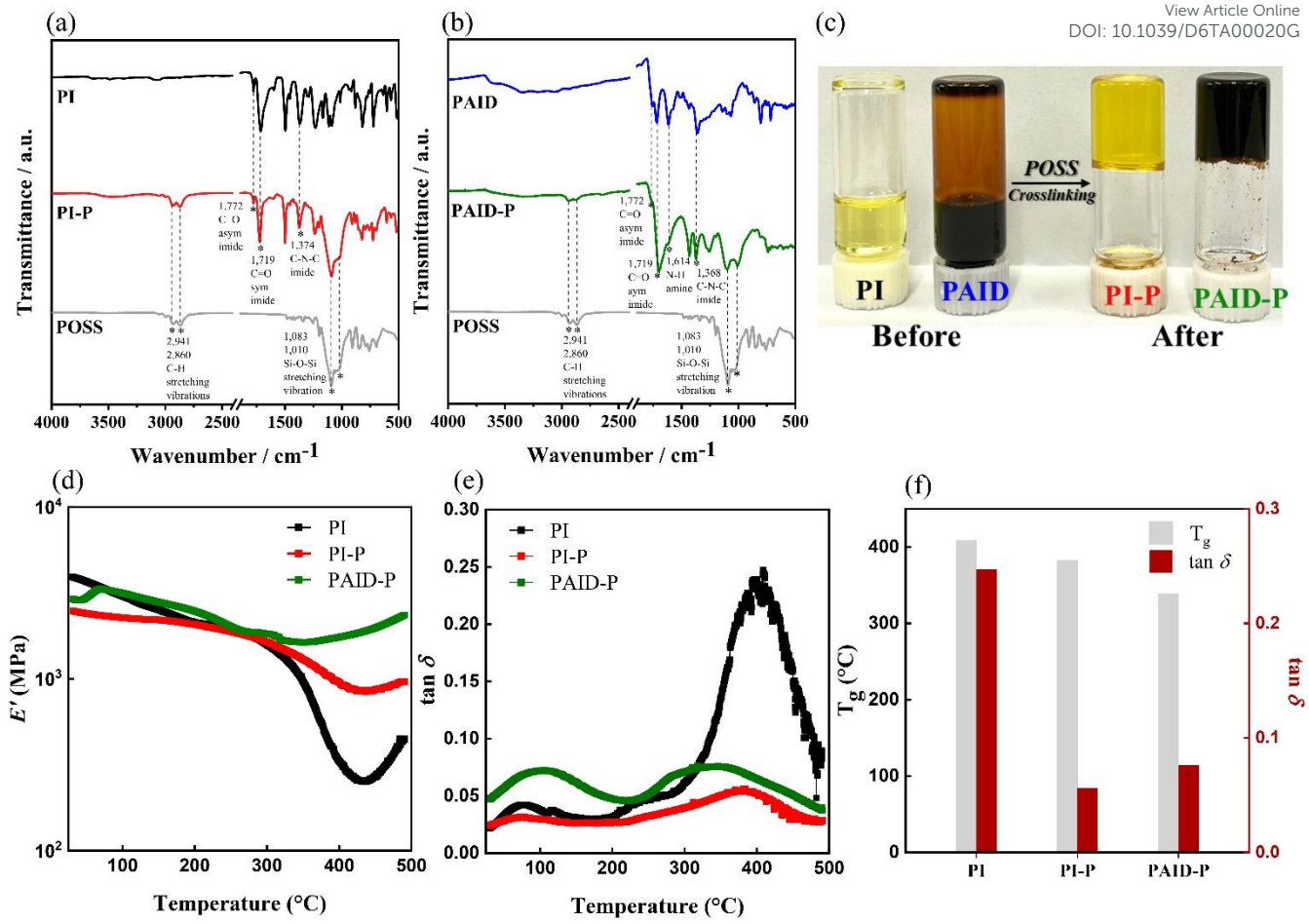

Fig 1 FT- IR spectra of (a) PI, PI-P polymers, and POSS, and (b) PAID, PAID-P polymers, and POSS. (c) Image of cross-linking reaction between polymers and POSS. (d) *E'*, (e) tan *δ* curves of PI, PI-P, and PAID-P free-standing films, and (f) comparison of T_g and tan *δ* peak values.

to strong secondary bonding interactions—such as dipole-dipole interaction and π-π stacking—enhance the binding properties of linear polymers. However, the repeated volume expansion and contraction of Si particles during cycling can potentially result in polymer chain slippage in the linear polymer binder system, weakening the adhesion between the polymer binder and Si particles, thereby resulting in irreversible volume recovery. To improve the secondary bonding interactions among the polymer chains, chemical crosslinking was introduced into the linear PI and PAID polymers employing oxirane-functionalized POSS as a crosslinker (Scheme 1). The abundant oxirane groups in the octafunctional POSS crosslinker undergo a ring-opening reaction when attacked by a nucleophilic nitrogen atom from the polymer backbone structure. In PI polymer, the weak nucleophilic amide groups react with oxirane-functionalized POSS to form a network structure. In contrast, the stronger nucleophilic amino groups in PAID polymer participate in a significantly effective crosslinking reaction with the oxirane-functionalized POSS (Scheme S1).

Fig. 1d shows the images of the PI-P and PAID-P polymers before and after curing, revealing the formation of a network structure. The PI-P and PAID-P polymers remained in the gel state and did not flow, indicating successful crosslinking with the oxirane-terminated POSS. The chemical structures of the PI, PAID, PI-P, and PAID-P polymers were determined via FT-IR. All samples were pretreated under vacuum conditions at 200 °C for 2 h. FT-IR spectra of the PI, PAID, PI-P, and PAID-P polymers exhibited the characteristic stretching peaks of C–N–C symmetric, C=O symmetric, and asymmetric stretching in imide groups at 1368–1374, 1719, and 1772 cm^{-1}, respectively. The PI-P and PAID-P polymers exhibited C–H stretching at 2850–2941 cm^{-1} and Si–O–Si stretching at 1083–1010 cm^{-1}, indicative of the POSS cross-linker (Fig. 1a and b) [32, 37, 38]. These results validate the crosslinked structures of the PI-P and PAID-P polymers. Furthermore, FT-IR spectra of the Si anode utilizing the PI-P and PAID-P binders exhibited a characteristic peak for the crosslinking of the binder (Fig. S3-S4), indicating that the 3D networking structures of PI-P and PAID-P binders were successfully created within the Si anodes. Cyclic voltammetry (CV) was conducted to evaluate the electrochemical stability of the polymer binders within the operating voltage range of 0.05-3.5 V (vs Li/Li^+) (Fig. S5). The cathodic and anodic peak currents of the PI, PAID, PI-P, and PAID-P binders were quite weak and exhibited similar to each other. Compared with the peaks observed in Si anodes with the binders (Fig. S5), their significantly lower current responses indicate that they are

View Article Online
DOI: 10.1039/D6TA00020G

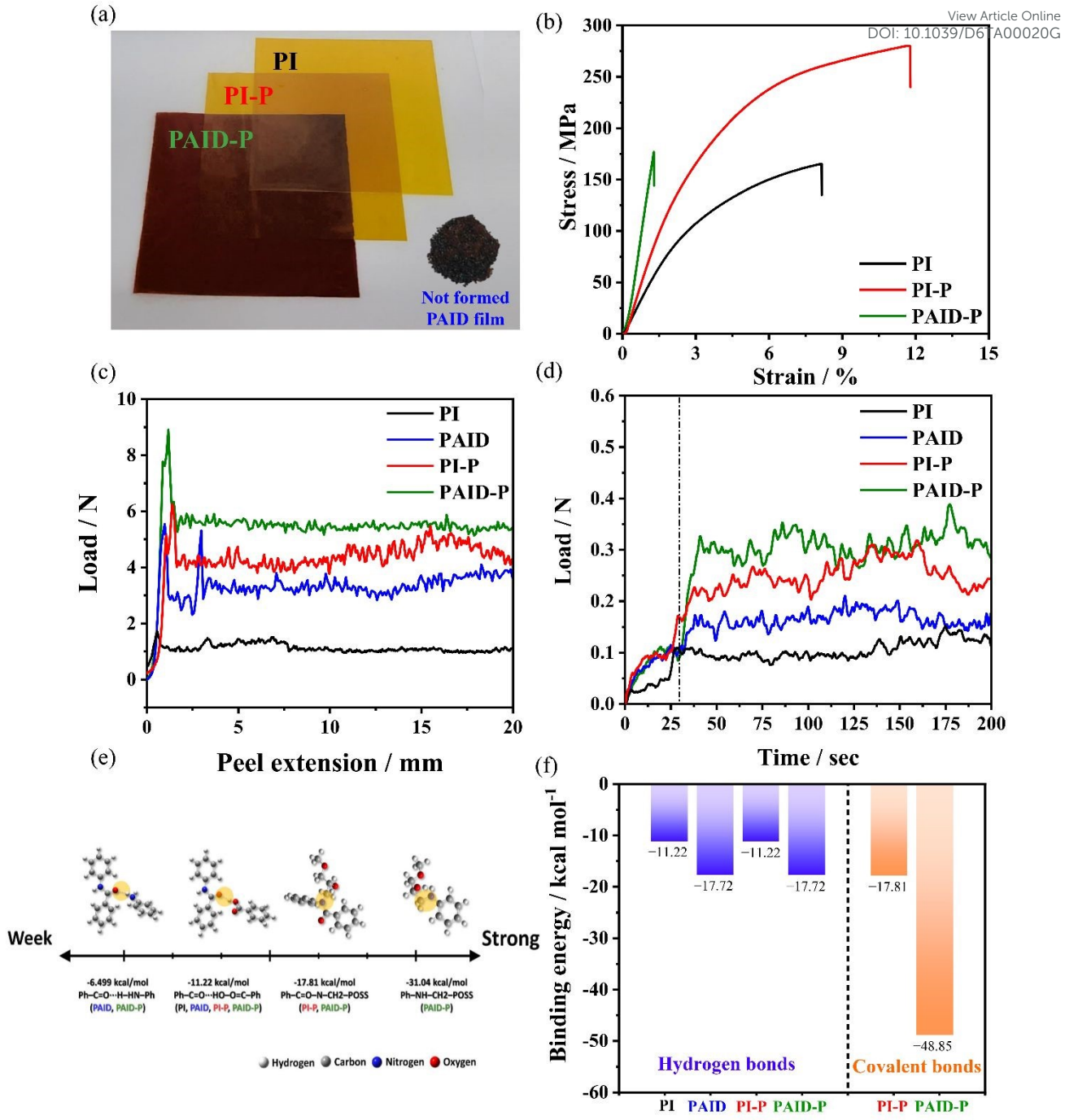

Fig 2 (a) Free-standing films of PI, PI-P, and PAID-P. (b) Stress-strain curves of corresponding free-standing films. (c) The peel test and (d) SAICAS data of Si anode with different binders. (e) the chemical bond formation in polymeric binders and corresponding binding energies calculated by DFT calculations. (f) Comparison of binding energy values.

electrochemically inert as Si anode binders. Thus, the synthesized polymer binders have negligible side reactions with the electrolyte, conductive additives, and current collectors. Notably, the crosslinking reactions between the polymers and oxirane-functionalized POSS prevented heterocyclic ring formation in the PI and PAID polymers (Scheme 1), thereby softening the backbones of both polymers and preventing excessive rigidity in the crosslinked polymers. This unique chemical crosslinking reaction exerted a significant effect on the stress–tensile behavior of the resulting freestanding polymer films (Fig. 2a). The hard-type PAID polymer was initially challenging to fabricate into a free-standing film owing to its brittleness; however, the incorporation of the POSS crosslinker diminished its brittleness, enabling the successful fabrication of a free-standing film. This demonstrates that POSS crosslinking enhances the flexibility of the polymer. The stress–strain curves of the freestanding films are presented in Fig. 2b. The tensile strengths of PI, PI-P, and PAID-P polymers were 165, 279, and 144 MPa, respectively, and their corresponding elongation rates were 8.1, 11.7, and 1.3%, respectively. The crosslinked PI-P

View Article Online DOI: 10.1039/D6TA00030G

polymer exhibited higher tensile strength and ductility than those of non-crosslinked PI polymer. POSS crosslinking enhanced the flexibility of the polymer while simultaneously increasing the tensile strength via network formation, thereby improving the toughness of the polymer. To verify the crosslinking-induced flexibilization effect, DMA measurements were performed on PI, PI-P, and PAID-P films. Generally, conventional crosslinking restricts segmental motion, resulting in a more rigid polymer network with an increased glass transition temperature (T_g) and a reduced loss tangent (tan δ). However, the POSS-crosslinked PI-P and PAID-P films exhibited distinctive DMA behavior. As shown in Fig. 1d-f, the T_g values of the PI-P (382.2 °C) and PAID-P (338.5 °C) films were lower than that of the PI film (408.8 °C), indicating that the flexible and spherical POSS crosslinkers hinder tight chain packing and increase the free volume of the polymer network. This strongly suggests that POSS crosslinking enhances the chain flexibility of polymer binders. Simultaneously, a sharp decrease in the tan δ peak value was observed for PI-P and PAID-P, confirming the formation of typical crosslinked polymer network. As a result, we demonstrated that POSS-based crosslinking effectively induces a flexibilization effect, enabling the coexistence of structural robustness and enhanced chain mobility.

Nanoindentation was conducted to evaluate mechanical integrity of Si anodes depending on binders (Fig. S11 and Table. S2). The indentation depths of the PI, PAID, PI-P, and PAID-P-based Si anodes were 4.44, 4.18, 2.24, and 2.26 μm, respectively, showing a significant decrease upon POSS incorporation. In addition, the reduced modulus (Er), determined using the Oliver–Pharr method, was 0.983, 1.58, 2.872, and 3.093 GPa, and the hardness (H) values were 0.022, 0.034, 0.089, and 0.090 GPa for PI, PAID, PI-P, and PAID-P, respectively, both following the order of PI < PAID < PI-P < PAID-P with a significant increase in the POSS-incorporated binders. These results strongly indicate that the POSS-based polymer network structure effectively enhances the mechanical integrity of the Si anodes. To evaluate the binding energies of the polymers with and without the crosslinker, the covalent bonding energies between the polymers and POSS crosslinker, as well as the hydrogen-bonding energies between the polymers, were calculated using DFT and the B3LYP/ 6-31G(d,p) basis set (Fig. 2e and f). The hydrogen bonding energies of PI and PAID polymers were −11.22 and −17.72 kcal mol^{-1}, respectively. The PAID polymer exhibited substantially stronger secondary bonding interactions compared with the PI polymer. The covalent bonding energies between oxirane POSS crosslinker and PI polymer, and between oxirane POSS crosslinker and PAID polymer were −17.81 and −31.04 kcal mol^{-1}, respectively. These results show that POSS crosslinked PAID-P polymer exhibits a more robust network binder structure than PI-P polymer. The bonding energies of the polymers gradually increased in the order of PI < PAID < PI-P < PAID-P. Overall, the PAID-P polymer improves both the primary and secondary interactions among the binders, providing enhanced durability against volume changes that occur during lithiation and delithiation.

The adhesion between the Si-binder composite layer and the Cu current collector is critical for the electrochemical performance of Si anodes. A 180° peel test and SAICAS were employed to compare the adhesion forces of Si anodes that utilize PI, PAID, PI-P, and PAID-P binders. The average adhesion force during the peel tests was determined from the crack point at a depth of 20 mm. Fig. 2c shows that the PI-P and PAID-P based Si anodes exhibit average adhesion forces of 4.2 and 5.4 N, respectively, outperforming the average adhesion forces of Si anodes that utilize PI (1.1 N) and PAID (3.9 N) binders. Furthermore, SAICAS data indicated that the average adhesion forces of the PI-P and PAID-P based Si anodes were 0.25 and 0.30 N, respectively, which were higher than those of the PI (0.10 N) and PAID (0.16 N) based Si anodes (Fig. 2d), respectively. SAICAS indicated nearly identical trend as that of the peel test. These analyses clearly demonstrate that the introduction of crosslinkers increased the average adhesion force of the Si anodes. Notably, the PAID-P-based Si anode exhibited enhanced adhesion properties than those of the Si anodes that utilize the PI-P binder.

Binder properties in Li-Ion Batteries

Fig. 3a depicts the initial charge-discharge voltage profiles of the Si anodes that utilize the PI, PAID, PI-P, and PAID-P binders, exhibiting the initial charge capacities (lithiation) of 3537, 3465, 3878, and 3915 mAh g^{-1}, respectively. The PAID-P-based Si anode exhibited the highest initial discharge capacity of 2820 mAh g^{-1} with initial Coulombic efficiency (ICE) of 72%, followed by Si anodes that utilize PI (2108 mAh g^{-1}, 60%), PAID (2550 mAh g^{-1}, 72%), and PI-P (2648 mAh g^{-1}, 69%) binders. The improved capacity and ICE of the Si anodes with POSS crosslinked binders (PI-P and PAID-P) are attributed to their 3D network structure, which reduces their inherent rigidity and dissipates the stress of Si expansion during initial lithiation. Furthermore, the superior performance of PAID-P over PI-P is attributed to strong secondary bonding with the Si particles and enhanced intermolecular interactions within the binders (Scheme 1). Fig. 3b presents the cycling performance of the Si anodes over 200 cycles at a rate of 0.2 C. The discharge capacity of the PI-based Si anode decreased rapidly during the initial 50 cycles and retained 27% of its initial capacity (166 mAh g^{-1}) after 200 cycles, whereas PAID, PI-P and PAID-P-based Si anodes exhibited superior capacity retention, maintaining more than 65% of the initial capacity after 200 cycles. Among these binders, the PAID-P-based Si anode maintained the highest discharge capacity of 1881 mAh g^{-1} over 200 cycles. The rate capability tests were conducted to know the impact of POSS crosslinker on the electrochemical kinetics of Si anode (Fig. 3c). Additionally, at high charge current density of 1C, Si anodes showed different cycle performance during 150 cycles (Fig. S7-8) depending on the POSS-crosslinking. The PI and PAID-based Si anodes showed drastic capacity fading during the first 50 cycles. On the other hand, PI-P and PAID-P-based Si anodes exhibited much higher discharge capacities of 1456 and 1664 mAh g^{-1}, with retention rates of 59%, outperforming the PI and PAID-based Si anodes (150 mAh g^{-1}, 7% retention and 1149 mAh g^{-1}, 48% retention), respectively. At all current densities from 0.2 C to 15 C, the discharge capacity was higher in order of PI, PAID, PI-P, and PAID-P-based Si anodes. At high current density of 15 C, Si

View Article Online
DOI: 10.1039/D6TA00020G

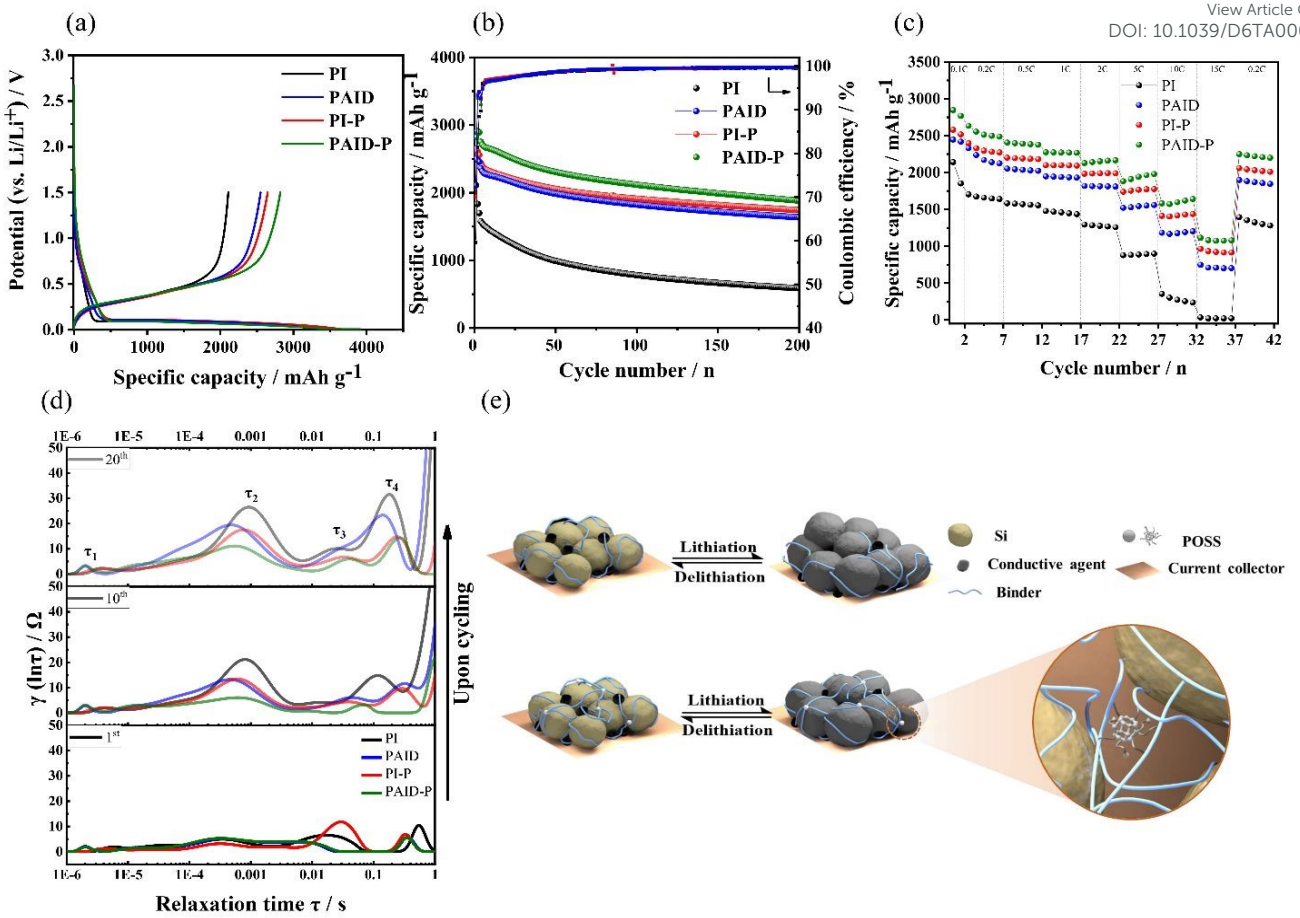

Fig 3 (a) The charge-discharge voltage profiles, (b) electrochemical cycle performance Si anode with different binders at current density of 0.2C. (c) rate capability test at different current densities. (d) DRT results of EIS data for Si anode with different binders after the 1st, 10th, and 20th cycles. (e) Schematic 3D illustration of Si anode during cycling and chemical bond formation of polymeric binders.

anodes with PI-P and PAID-P (915 and 1074 mAh g^{-1}) showed a relatively higher discharge capacity than those with PI and PAID binders (21 and 702 mAh g^{-1}). The POSS structure, with four oxygen atoms on a single face, forms a pseudo-crown ether configuration, allowing it to act as a Lewis base, coordinate with Li^+ cations, and facilitate efficient ion transportation [39-41]. These characteristics of POSS effectively influenced the electrochemical kinetics for alloying reaction of Si with lithium. Fig. 3d shows distribution of relaxation time (DRT) analysis results, which is calculated the time characteristics obtained through electrochemical impedance spectroscopy (EIS). The DRT method enables more precise identification of the key electrochemical processes from the overlapped semicircles in EIS spectra (Fig. S10), simplifying impedance analysis and allowing the interpretation of electrochemical kinetic properties within various time domains [42]. The first peak (τ_1) is attributed to the contact impedance between the Si composite and the current collector, the τ_2 peak corresponds to the solid electrolyte interface (SEI) layer, and the τ_3 and τ_4 peaks are associated with charge-transfer resistance [43, 44]. Si anodes based on PI-P and PAID-P with a POSS crosslinker showed a decrease in the τ_2 peak corresponding to the SEI layer and the τ_3 and τ_4 peaks associated with charge transfer upon cycling. In contrast, Si anodes with PI and PAID binders showed relatively higher τ_2, τ_3, and τ_4 peaks. To further investigate the interfacial characteristics, XPS analysis was performed on the cycled Si anode after 200 cycles to quantitatively compare the SEI composition (Fig. S12 and Table S3). The relative fractions of key SEI components were analyzed through deconvolution of the C 1s and F 1s spectra. In the C 1s region, the fraction of Li_2CO_3 decreased in the order of PI (18.4%) > PAID (15.2%) > PI-P (9.37%) > PAID-P (6.34%). In contrast, F 1s analysis revealed that the corresponding LiF fractions were 43.2%, 29.0%, 69.0%, and 54.6%, respectively, indicating that the POSS-incorporated Si anodes form a more LiF-rich SEI. In general, a relatively high accumulation of Li_2CO_3 in the SEI is associated with incomplete interfacial formation and continuous electrolyte decomposition. On the other hand, a LiF-rich SEI layer is widely recognized as mechanically robust and electrochemically stable. Therefore, the lower Li_2CO_3 fraction and higher LiF fraction observed in the PI-P- and PAID-P-based Si anodes indicate the formation of a more stable and durable SEI, highlighting the critical role of POSS incorporation in stabilizing the interphase. These results reveal that the introduction of POSS not only improves the mechanical stability of Si electrode through a 3D network structure but also facilitates effective charge transfer via the POSS structure with four oxygen atoms on a single face. To investigate the effect of the binder on the microstructure of Si

View Article Online
DOI: 10.1039/D6TA00020G

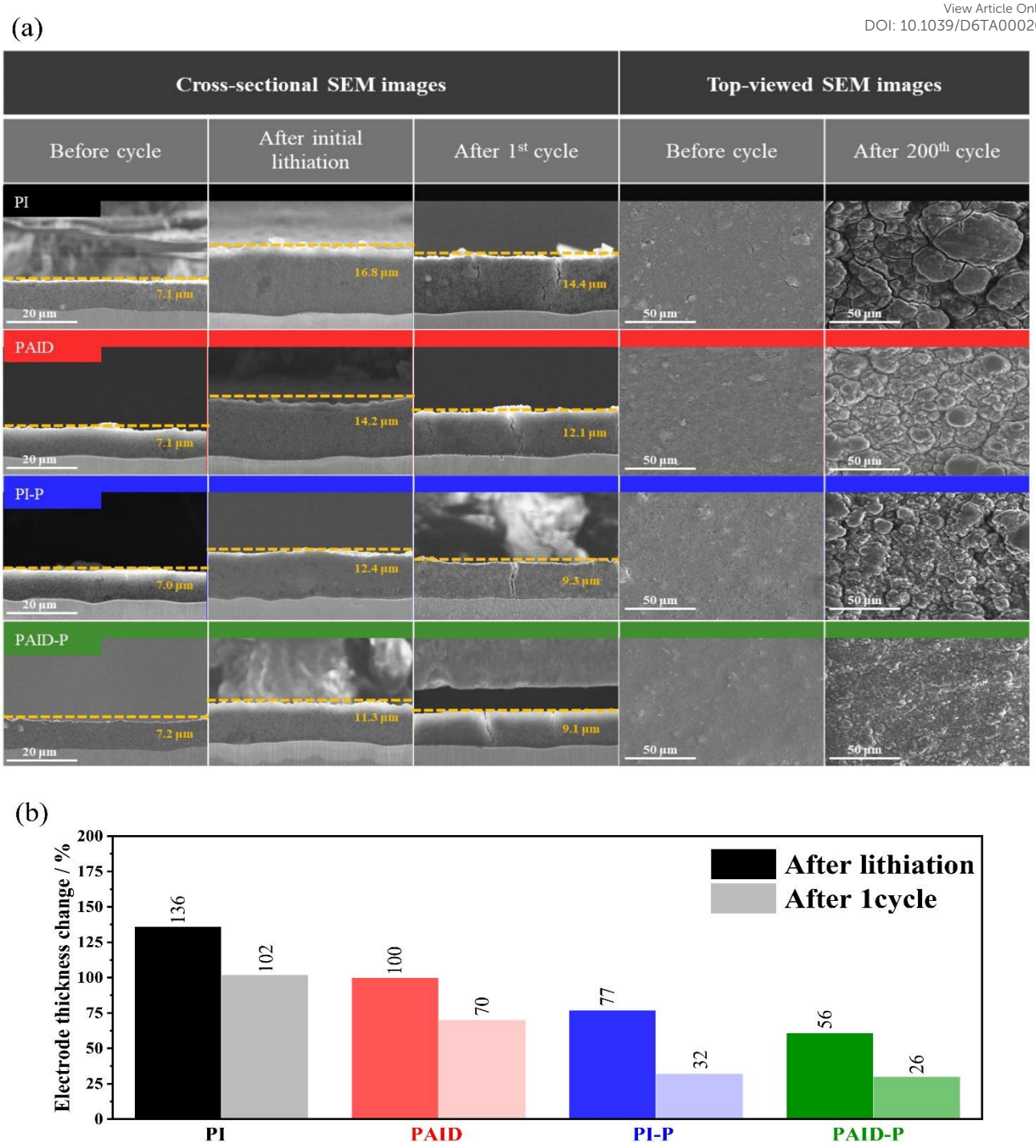

Fig 4 (a) Cross-sectional and top-viewed SEM images of PI-Si anode, PAID-Si anode, PI-P-Si anode, and PAID-P-Si anode before cycling, after initial lithiation, and after 1st cycle. (b) electrode thickness changes corresponding to SEM images.

anodes, pore characteristics were analyzed using mercury intrusion porosimetry (Fig. S13 and Table S4). The POSS-incorporated PI-P and PAID-P based Si anodes showed a decreased total pore area and increased pore diameters compared to the PI and PAID based Si anodes. This indicates the reduced internal surface area and enlarged pore structure. Among them, the PAID-P based Si anode maintains moderate porosity (19.75%) with reduced surface area and larger pore size, suggesting a more balanced pore structure. In contrast, the PI- and PAID-based Si anodes (23.42 and 27.63%) showed higher porosity and surface area, which may promote excessive interfacial side reactions, such as electrolyte decomposition and unstable SEI formation. Fig. 3e shows a schematic 3D illustration of the Si anodes with and without the POSS crosslinker during lithiation and delithiation. The POSS crosslinker reduces the spatial distance between the polymer binder chains, promoting strong interactions between functional groups, such as amines, amides, and carboxylic acids with Si particles. These strong

View Article Online
DOI: 10.1039/D5TA09206C

interactions between the Si particles and the functional groups of the binder minimize both the volume changes and structural deformation of the Si anodes, thereby enhancing the mechanical integrity of the Si anode during cycling. This is further corroborated by stress–strain curves, peel tests, and nanoindentation of the Si electrodes (Fig. 2b,c and S11). Consequently, the introduction of the POSS crosslinker improves the electrochemical properties of the Si anode, particularly in terms of reversible capacity and cycle stability.

Cross-sectional SEM images were obtained to investigate the capability of the binders to accommodate volume expansion and contraction of the Si composites during charging and discharging. Fig. 4a and b show SEM images of Si anodes before cycling, after initial lithiation, and after one cycle. The PI, PAID, PI-P, and PAID-P-based Si anodes expanded by 136%, 100%, 77%, and 56%, respectively, after the first full lithiation, and contracted by 102%, 70%, 32%, and 26%, respectively, after delithiation compared with their initial thickness. Following lithiation, the PI-P and PAID-P-based Si anodes exhibited less expansion than the PI and PAID-based Si anodes. This comparison indicates that the 3D network structures of the PI-P and PAID-P binders suppressed the volume changes of the Si electrodes more effectively. Likewise, during delithiation, the PI-P- and PAID-P-based Si anodes exhibited improved contraction than the PI and PAID-based anodes, revealing that these 3D network structures strengthened the secondary bonding within the polymer chains and prevented structural deformation of the Si electrode, thereby facilitating the contraction of the Si anodes. The volume recovery percentage of the Si electrodes was calculated as the ratio of the thickness of the Si anode after the first full delithiation to that after the first full lithiation. The volume recovery percentages of the PI, PAID, PI-P, and PAID-P-based Si anodes were 25, 30, 58, and 57%, respectively. The PI-P and PAID-P-based Si anodes exhibited superior volume recovery exceeding 57%, primarily owing to smaller volume expansion during lithiation and significant contraction during delithiation. On the other hand, the PI and PAID-based Si anodes exhibited lower volume recovery of 25% and 30%, respectively. Si anodes with and without POSS crosslinker also showed morphological differences in their top-viewed SEM images after 200cycles. Si anodes with PI and PAID binders showed severe surface cracking, whereas those with PI-P and PAID-P binders exhibited relatively more uniform morphology. These results indicate that the POSS crosslinked binder system shows excellent mechanical resilience, facilitated by a flexible 3D network structure as well as strong intermolecular interactions between the Si particles and conductive agents. These observations are consistent with the electrochemical performance and mechanical properties of the polymer binders. Furthermore, previously reported polyimide-derivative binders for Si anodes have primarily focused on improving solubility, introducing carboxyl groups, or tuning the rigidity–flexibility balance through the incorporation of flexible segments (Table S5). Conversely, this study is distinguished by the first introduction of crosslinking into polyimide binders, effectively overcoming the intrinsic brittleness of rigid aromatic polyimides while preserving the network structure. PI-P and PAID-P-based Si anodes utilizing the POSS crosslinker exhibited higher reversible capacities and long-term cycling stability, resulting in the best overall performance, consistent with the mechanical properties, peel test, SAICAS analysis, nanoindentation, and DFT calculations.

Conclusions

We proposed a crosslinking-induced flexibilization strategy on hard-type polyimide-based binders (PI-P and PAID-P) via in-situ crosslinking of PI and PAID binders with oxirane-functionalized POSS as a crosslinker for Si anodes in LIBs. The incorporation of POSS crosslinkers significantly enhanced the flexibility of the polymer backbone, complementing the inherent rigidity of the network structures of the PI-P and PAID-P binders. This modification not only prevents excessive rigidity of the cured polymers but also significantly improves their mechanical properties, thereby preventing polymer chain slippage and ensuring high stability of the electrode microstructure. During lithiation, the introduction of the POSS crosslinker effectively suppressed the volume expansion of the Si anode and substantially improved the volume recovery to its initial state. Consequently, PI-P and PAID-P-based Si anodes (crosslinked) demonstrated significantly improved electrochemical performance, exhibiting a higher reversible capacity and enhanced cycling stability over 200 cycles at a rate of 0.2 C compared with those of PI and PAID-based anodes. Notably, this crosslinking system demonstrated superior performance for both the conventional hard-type PI polymer structure as well as the more rigid PAID polymer structure, forming a robust 3D network structure without introducing excessive brittleness. The proposed crosslinking approach is expected to be applicable to other polymer binders based on epoxy–amine chemistry, where it can partially interfere with the formation of rigid polymer structures. This provides new insights into strategies for enhancing the performance of Si-based anodes in LIBs.

Author contributions

Junho Kim: Writing–original draft, Visualization, Validation, Methodology, Formal analysis, Data curation, Investigation. Gyuri Kim: Writing – original draft, Visualization, Validation, Methodology, Formal analysis, Data curation, Investigation. Ji Young Kim: Visualization, Methodology, Investigation. Sohyun Kim: Methodology, Investigation. In Hwan Jung: Writing – review & editing, Validation, Supervision, Resources, Funding acquisition, Data curation, Conceptualization. Hansu Kim: Writing – review & editing, Validation, Supervision, Resources, Funding acquisition, Data curation, Conceptualization.

Conflicts of interest

There are no conflicts to declare

Data availability

The data supporting this article have been included as part of the supplementary information (SI)

Acknowledgements

J. Kim and G. Kim contributed equally to this work. This work was supported by the National Research Foundation of Korea (NRF) grant funded by the Korean government (MSIT) (NRF-2021M3H4A1A02045967 and RS-2026-25491467).

References

1. S. Choi, T.-w. Kwon, A. Coskun and J. W. Choi, *Science*, 2017, **357**, 279-283.
2. H. Shobukawa, J. Shin, J. Alvarado, C. S. Rustomji and Y. S. Meng, *J Mater Chem A*, 2016, **4**, 15117-15125.
3. X. Han, Z. Zhang, H. Chen, L. Luo, Q. Zhang, J. Chen, S. Chen and Y. Yang, *J Mater Chem A*, 2021, **9**, 3628-3636.
4. W. Kim, D. Shin, B. Seo, S. Chae, E. Jo and W. Choi, *ACS nano*, 2022, **16**, 17313-17325.
5. D. Kim, M. Bae, S. J. Hwang, Y. Chang, Y. Kim, W. Y. An and Y. Piao, *J Mater Chem A*, 2025, **13**, 35354-35367.
6. J. Peng, R. Shao, S. Huang, Z. Cao, T. Zhang, Y. Cao, S. Zhang, C. Xu, Y. Shi and J. Niu, *J Mater Chem A*, 2022, **10**, 23008-23014.
7. S. Park, M. Choi, J. Lee, S. Lee, J. Kim, T. Yun, N. Kim, J. Sung, J. Cho and M. Ko, *Small*, 2025, **21**, 2404949.
8. A. N. Preman, H. Lee, J. Yoo, I. T. Kim, T. Saito and S.-k. Ahn, *J Mater Chem A*, 2020, **8**, 25548-25570.
9. Z. Cao, X. Zheng, Q. Qu, Y. Huang and H. Zheng, *Advanced Materials*, 2021, **33**, 2103178.
10. J. Moon, H. C. Lee, H. Jung, S. Wakita, S. Cho, J. Yoon, J. Lee, A. Ueda, B. Choi and S. Lee, *Nat Commun*, 2021, **12**, 2714.
11. X. Shan, Z. Cao, G. Zhu, Y. Wang, Q. Qu, G. Liu and H. Zheng, *J Mater Chem A*, 2019, **7**, 26029-26038.
12. X. Jiao, J. Yin, X. Xu, J. Wang, Y. Liu, S. Xiong, Q. Zhang and J. Song, *Advanced Functional Materials*, 2021, **31**, 2005699.
13. H. Chen, Z. Wu, Z. Su, S. Chen, C. Yan, M. Al-Mamun, Y. Tang and S. Zhang, *Nano Energy*, 2021, **81**, 105654.
14. V.-P. Vu, H.-M. So, A. Kim, J. Y. Lee, M. Oh and S. Hyun, *J Mater Chem A*, 2025, **13**, 38541-38571.
15. D. Cheng, F. Song, Y. Zeng, D. Qin, Z. Ma, P. Zheng, G. Zhang, C. Wang and Y. Qian, *Advanced Functional Materials*, 2025, **35**, 2507041.
16. J. Kang, J. Y. Kwon, D.-Y. Han, S. Park and J. Ryu, *Applied Physics Reviews*, 2024, **11**.
17. Z. Deng, J. Xu, C. Shi, J. Lai, H. Dong, M. Wang, B. Hong and Y. Lai, *ACS Applied Polymer Materials*, 2025, **7**, 9131-9141.
18. D. Y. Han, I. K. Han, J. Son, J. Y. Kwon, Y. S. Kim, T. K. Lee, S. Park and J. Ryu, *Advanced Functional Materials*, 2025, **35**, e09445.
19. W. Tan, B. Liang, M. Chen, H. Xiao, X. He, W. Yang, J. Hu, K. Zeng and G. Yang, *Chemical Engineering Journal*, 2024, **496**, 153822.
20. M. A. Elnaggar, N. Dong, Y. Kang, B. Liu, D. Lin, G. Tian, S. Qi and D. Wu, *J Mater Chem A*, 2025.
21. X. Li, J. He, Y. Liao, S. Zhu, Y. Tang, H. Li, N. Lv, Y. Xu and Y. Wang, *J Power Sources*, 2022, **525**, 231124.
22. Y. Xu, Q. Zhang, N. Lv, H. Li, Z. Wei, Y. Wang and H. Tang, *Energ Fuel*, 2023, **37**, 2441-2448.
23. J. Kim, G. Kim, Y. K. Park, G. Lim, S. T. Kim, I. H. Jung and H. Kim, *Advanced Functional Materials*, 2023, **33**, 2303810.
24. Y. J. Kwon, J.-O. Kim, E. Vivek, E. Kim, S. H. Kim, T. Kwon, E. Lim, S. Chae, M. Park and Y. Eom, *Chemical Engineering Journal*, 2024, **479**, 147860.
25. X. Wan, T. Mu, B. Shen, Q. Meng, G. Lu, S. Lou, P. Zuo, Y. Ma, C. Du and G. Yin, *Nano Energy*, 2022, **99**, 107334.
26. C. Liang, Z. Li, T. Chen, Q. Wang, R. Guo and Y. Liu, *Reactive and Functional Polymers*, 2026, 106680.
27. X. Hou, Y. Mao, R. Zhang and D. Fang, *Chemical Engineering Journal*, 2021, **417**, 129341.
28. H. Guo, L. Liu, Y. Yu, Q. Zhang, Q. Chang and Y. Liu, *J Power Sources*, 2025, **640**, 236629.
29. L. Gautam, S. G. Warkar, S. I. Ahmad, R. Kant and M. Jain, *Polymer engineering & science*, 2022, **62**, 225-246.
30. S. Askari, M. M. Hamedi and O. Sevastyanova, *J Energy Storage*, 2025, **115**, 115838.
31. W. Shen, B. Du, H. Zhuo and S. Chen, *Chemical Engineering Journal*, 2022, **428**, 132609.
32. H. Yang, C. He, T. P. Russell and D. Wang, *Giant-Amsterdam*, 2020, **4**, 100035.
33. K. Zhang, D. Zhang, Z. Zhang, Y. Wu, X. Bi and R. Yang, *ACS Applied Polymer Materials*, 2025, DOI: 10.1021/am101123h.
34. S. Morsch, C. R. Wand, S. Gibbon, M. Irwin, F. Siperstein and S. Lyon, *Applied Surface Science*, 2023, **609**, 155380.
35. J. Kim, Y. K. Park, H. Kim and I. H. Jung, *Chem Mater*, 2022, **34**, 5791-5798.
36. M. Konáš, T. M. Moy, M. E. Rogers, A. R. Shultz, T. C. Ward and J. E. Mcgrath, *Journal of Polymer Science Part B: Polymer Physics*, 1995, **33**, 1429-1439.
37. C. Ramírez, M. Rico, A. Torres, L. Barral, J. López and B. Montero, *European Polymer Journal*, 2008, **44**, 3035-3045.
38. K. Iida, Y. Imamura, C. Liao, S. Nakamura and G. Sawa, *Polym J*, 1996, **28**, 352-356.
39. P. R. Chinnam and S. L. Wunder, *Chem Mater*, 2011, **23**, 5111-5121.
40. E. C. Allen and K. J. Beers, *Polymer*, 2005, **46**, 569-573.
41. A. R. Polu and P. K. Singh, *Materials Today: Proceedings*, 2022, **49**, 3076-3080.
42. H. Yuan, W. Lin, C. Tian, M. Buga, T. Huang and A. Yu, *Nano-Micro Letters*, 2025, **17**, 288.
43. H. Jia, L. Zou, P. Gao, X. Cao, W. Zhao, Y. He, M. H. Engelhard, S. D. Burton, H. Wang and X. Ren, *Advanced Energy Materials*, 2019, **9**, 1900784.
44. A. S. Mehranjani, M. Golmohammad, S. Bozorgmehri and H. Abdoli, *J Power Sources*, 2024, **602**, 234356.

View Article Online
DOI: 10.1039/D6TA00020G

Data availability statements

The data supporting this article have been included as part of the Supplementary Information.